Electronic Supplementary Material (ESI) for Nanoscale.

Supporting Information

Magnetic Field Modulated SERS Enhancement of CoPt Hollow Nanoparticles with Size Below 10 nm

Yinong Wang[a,b], Qing Liu[a], Yinghui Sun[a] and Rongming Wang *[a]

a. Beijing Advanced Innovation Center of Materials Genome Engineering, and Beijing Key Laboratory for Magneto-Photoelectrical Composite and Interface Science, School of Mathematics and Physics, University of Science and Technology Beijing, Beijing 100083, China.

b. Department of Physics, Beihang University, Beijing 100191, China

** Corresponding Author. E-mail: rmwang@ustb.edu.cn*

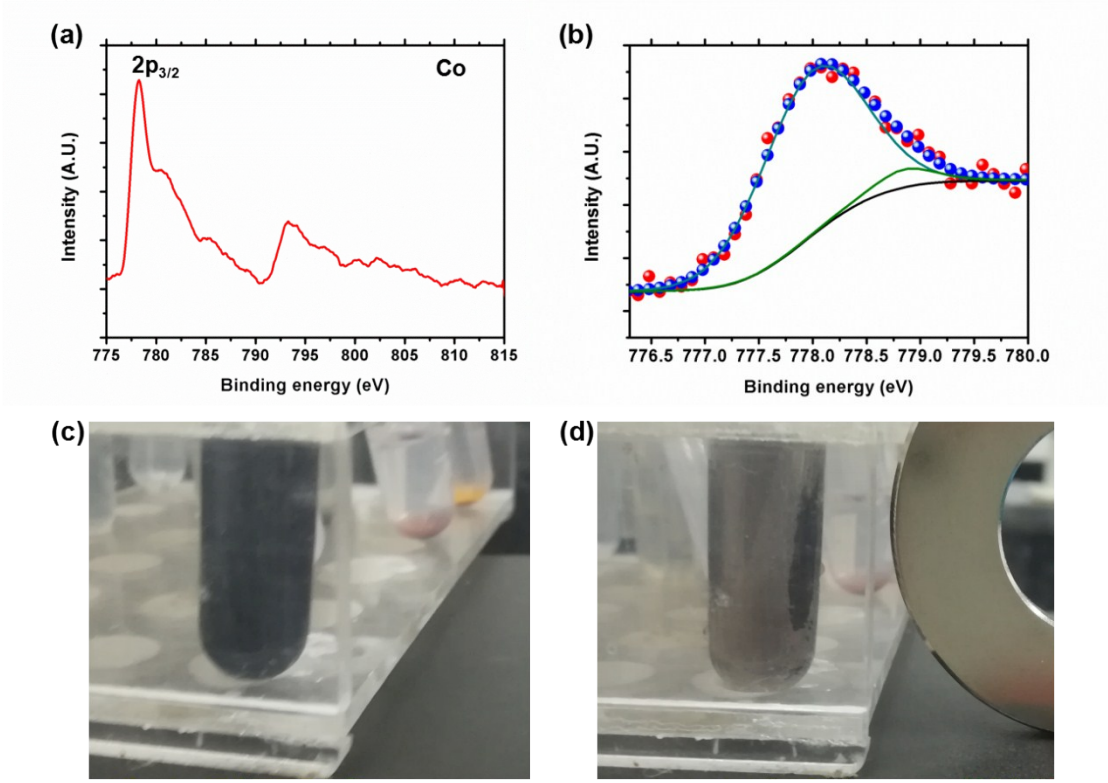

Fig. S1. (a) XPS spectrum of Co 2p for as-prepared samples. (b) The fitting of Co $2p_{3/2}$ XPS peak. (c) Uniform CoPt hollow NPs solution. (d) The CoPt hollow NPs solution after exposure to an external magnetic field.

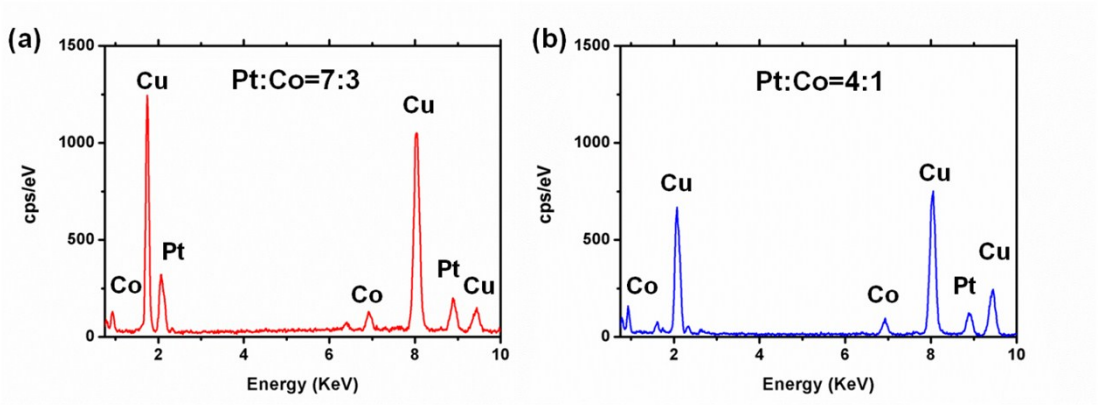

Fig. S2. (a) EDS of CoPt hollow NPs revealing the atomic ratio of Pt to Co as 7:3. (b) EDS of CoPt hollow NPs etched by 1 mol/L HCl solution, revealing the atomic ratio of Pt to Co as 4:1.

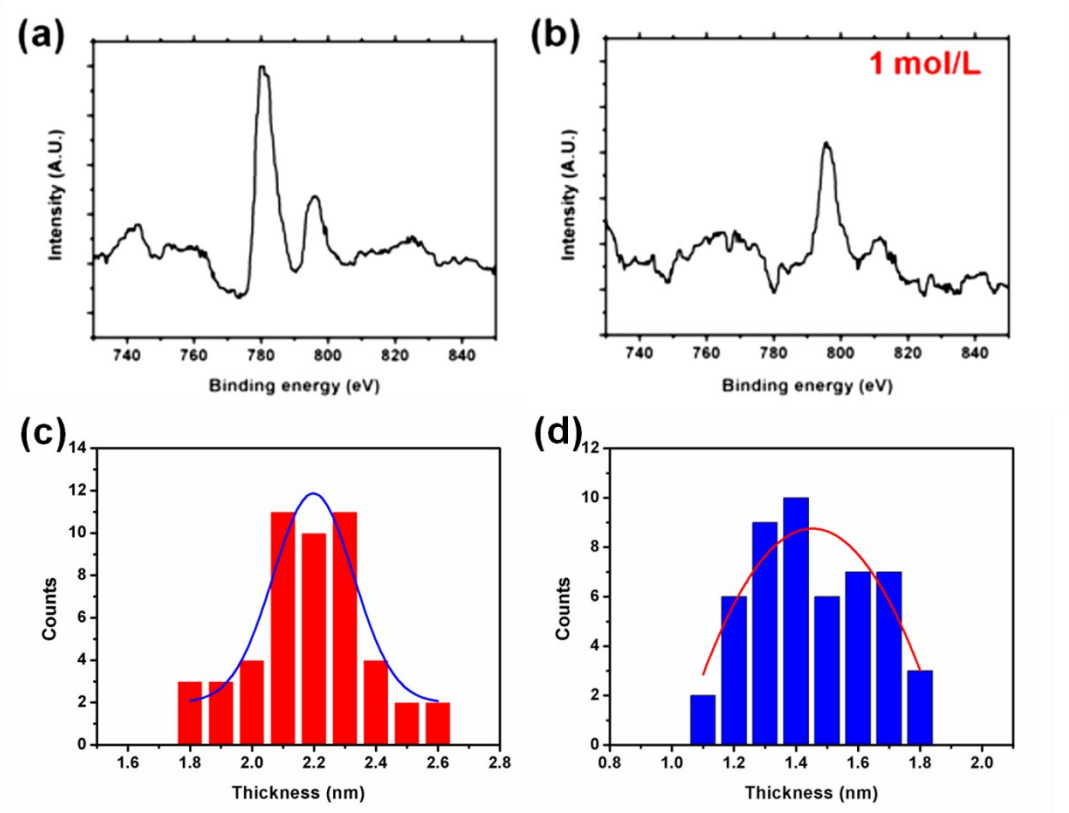

Fig. S3. (a) The Co element EELS spectrum of the CoPt hollow NPs. (b) The Co element EELs spectrum of the HCl-etched CoPt hollow NPs. (c) Shell thickness distribution histograms of CoPt hollow NPs. (d) Shell thickness distribution histograms of HCl-etched CoPt hollow NPs.

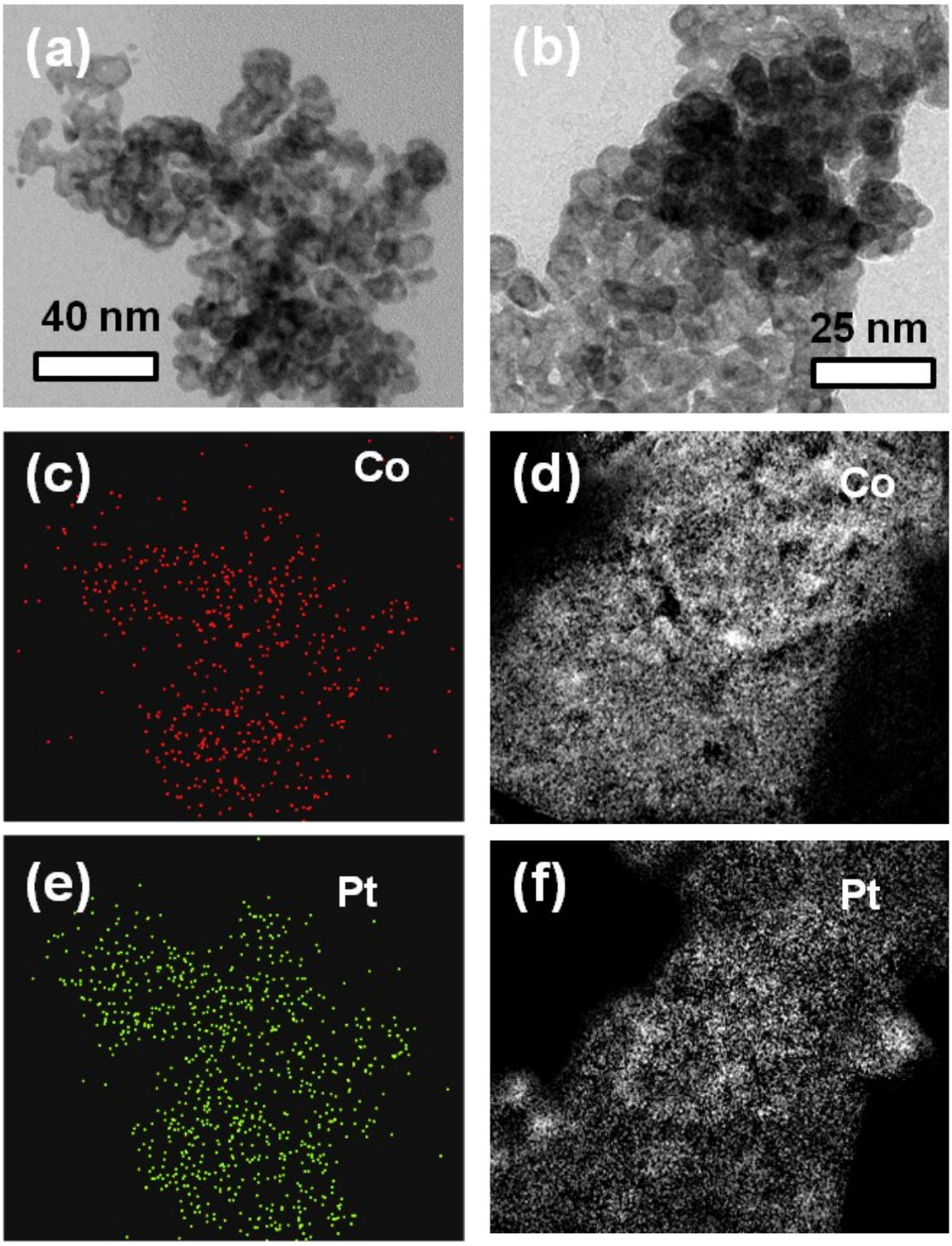

Fig. S4. (a) and (b) TEM images of CoPt hollow NPs. (c) and (e) STEM-EDS mapping of Pt and Co from the area in (a). (d) and (f) the STEM-EELs mapping of Pt and Co from the area in (b).

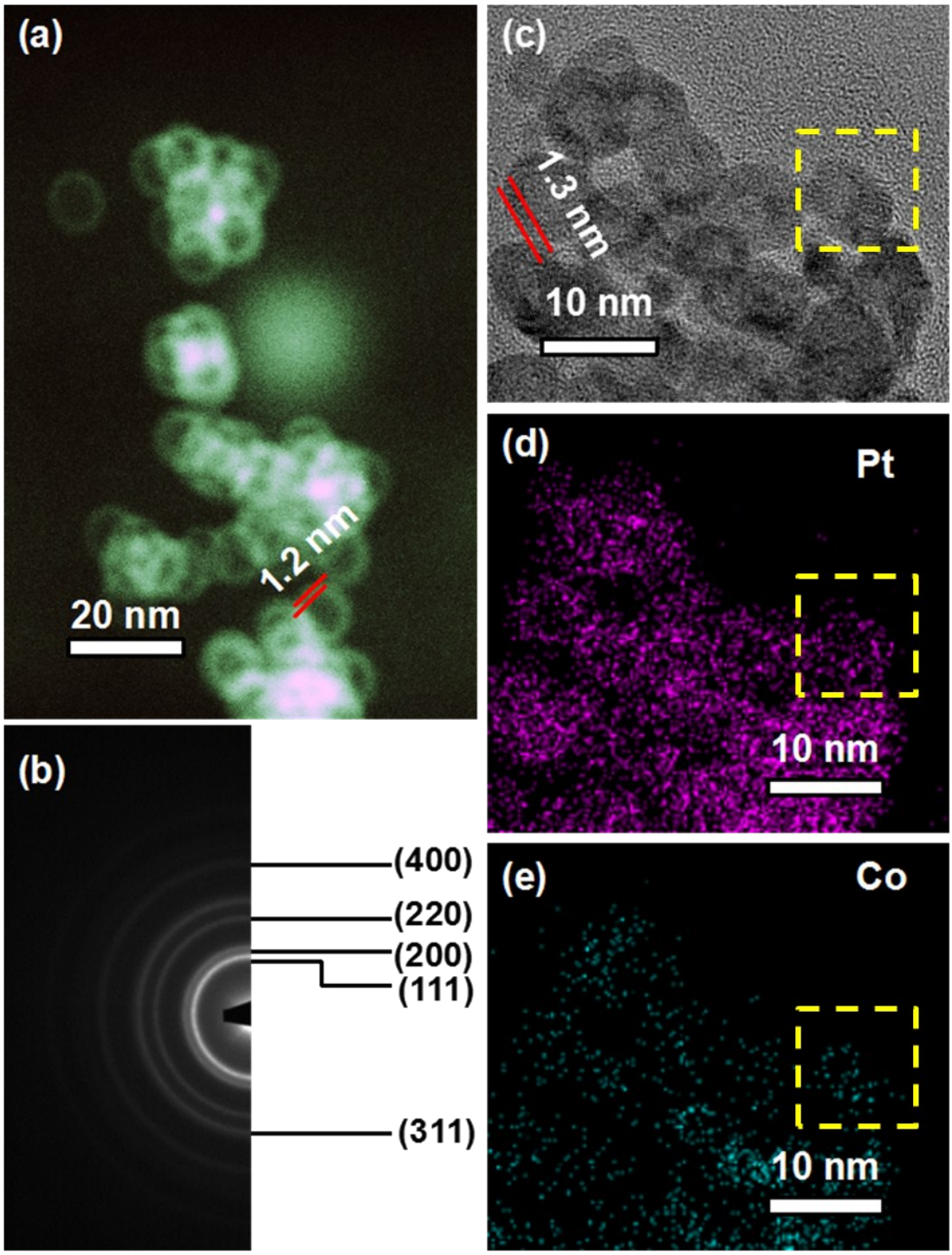

Fig. S5. HCl-treated CoPt hollow NPs. (a) STEM image; (b) Electron diffraction; (c) TEM image; (d) and (e) STEM-EDS mapping of Pt and Co from the area in (c).

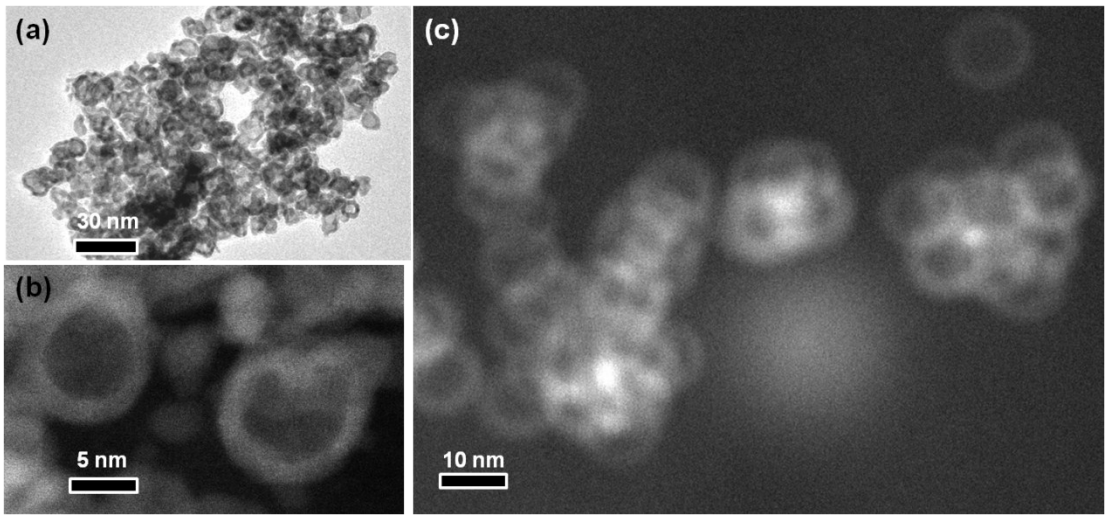

Fig. S6. (a) The TEM image of as-prepared CoPt hollow NPs. (b) The STEM image of as-prepared CoPt hollow NPs. (c) The STEM image of the HCl-treated CoPt hollow NPs.

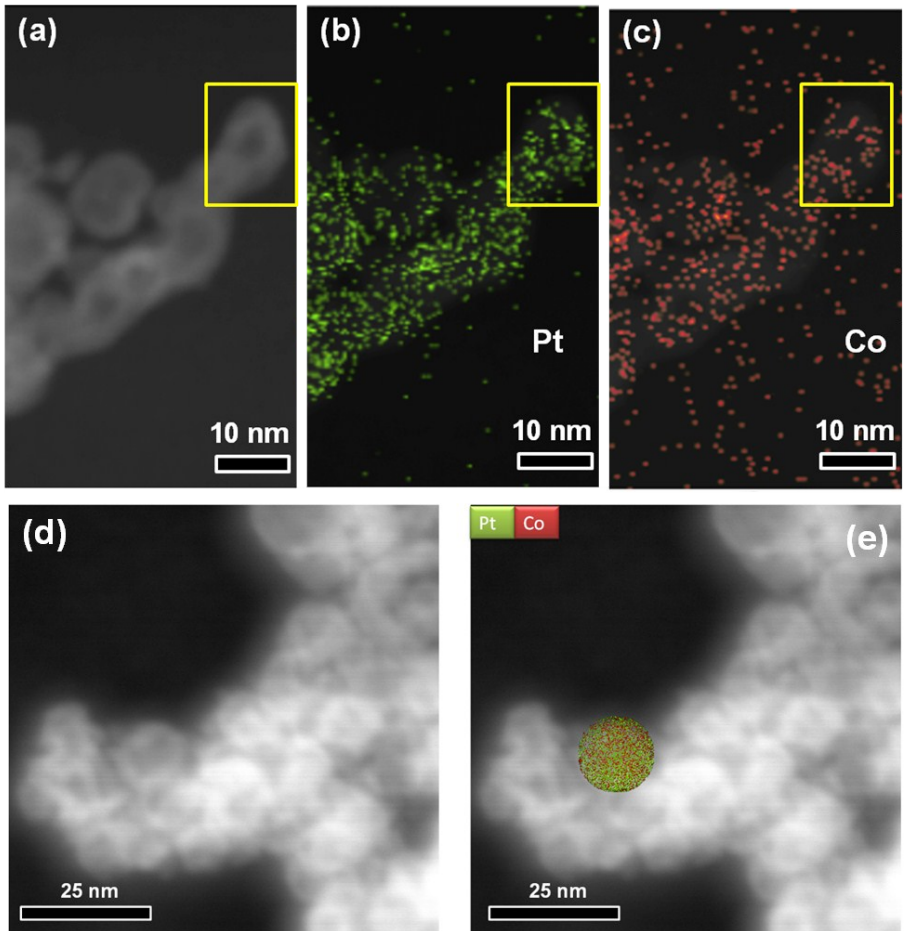

Fig. S7. (a) and (d) STEM images of CoPt hollow NPs without HCl treatment. (b) and (c) STEM-EDS mapping of Pt and Co from the selected area in (a). (e) EDS elemental mapping for the selected circular area of (d), revealing Co and Pt distribution in CoPt hollow NPs. (e) EDS elemental mapping for the selected area of (d) in a circle, revealing Co and Pt distribution in CoPt hollow NPs.

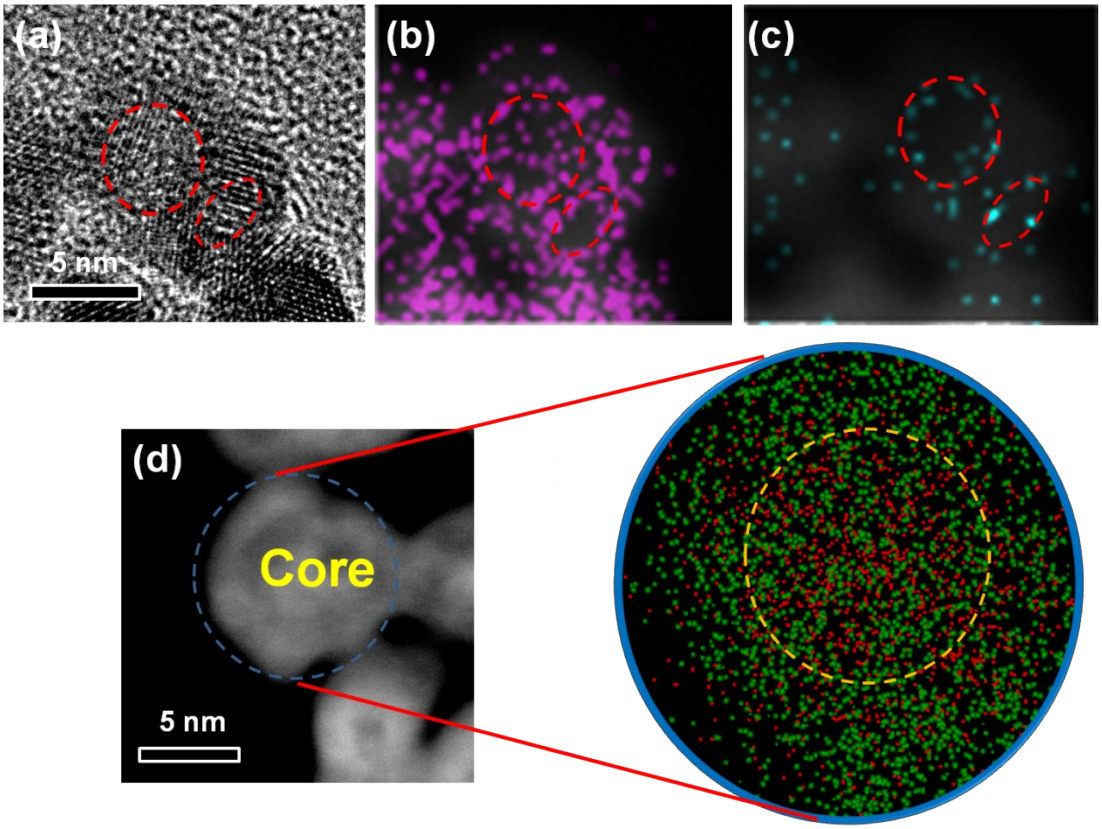

Fig. S8. The Co and Pt distribution in HCl-treated CoPt hollow NPs. (a) and (d) TEM and STEM image of CoPt hollow NPs with HCl treatment. (b) and (c) STEM-EDS mapping of Pt and Co from the selected area in (a), corresponding to the yellow selected area of Figs. S5 (d) and (e). The inset of (d) is the EDS elemental mapping for the selected circular area of (d), revealing Co and Pt distribution in CoPt hollow NPs.

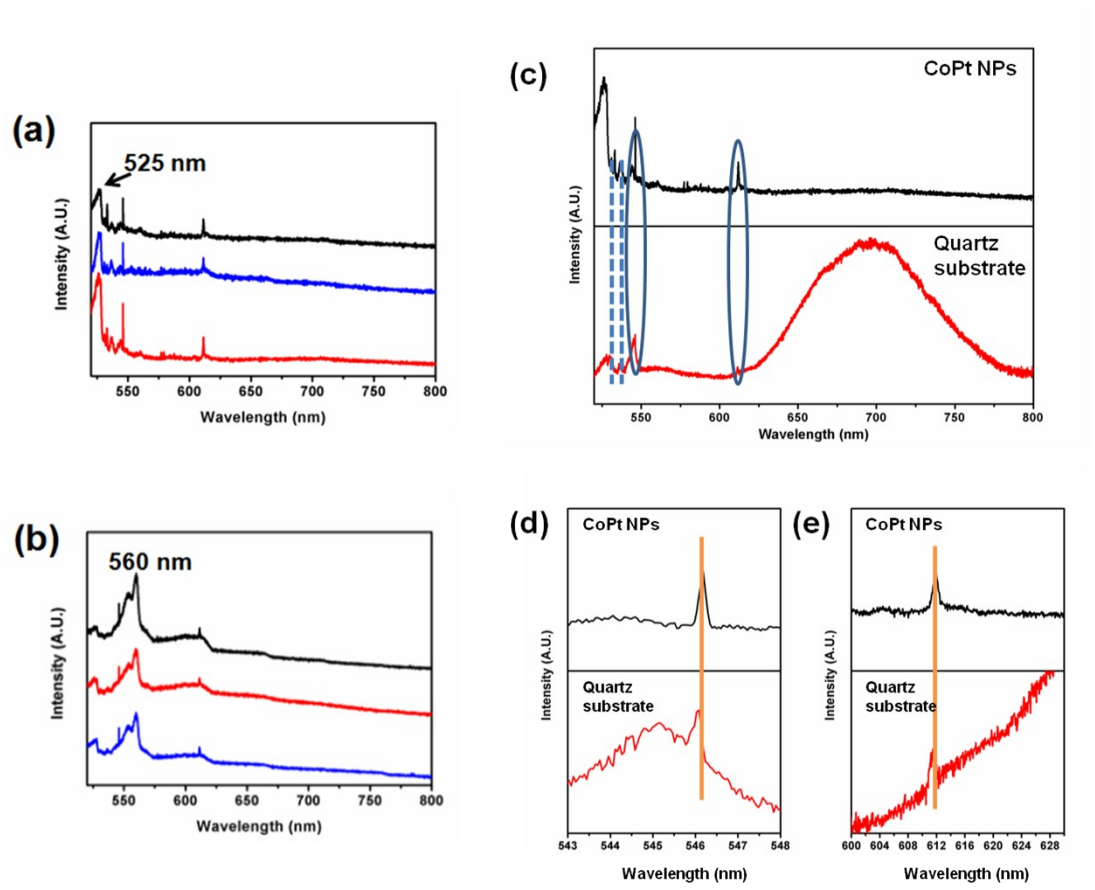

Fig.S9. Emission spectra collected from different regions of agglomerated CoPt hollow NPs on quartz. (a) As-prepared NPs; (b) NPs after HCl etching. (c) Emission spectra of CoPt hollow NPs (black line) and quartz substrate (red line). The emission peak at ~700 nm in the spectrum is a result of the amorphous structure of the quartz wafer substrate. In (d) and (e), emission spectra peaks are seen at ~550 nm and at ~610 nm, respectively. Again, the black lines are obtained from the CoPt samples and the red lines are from the quartz substrate.

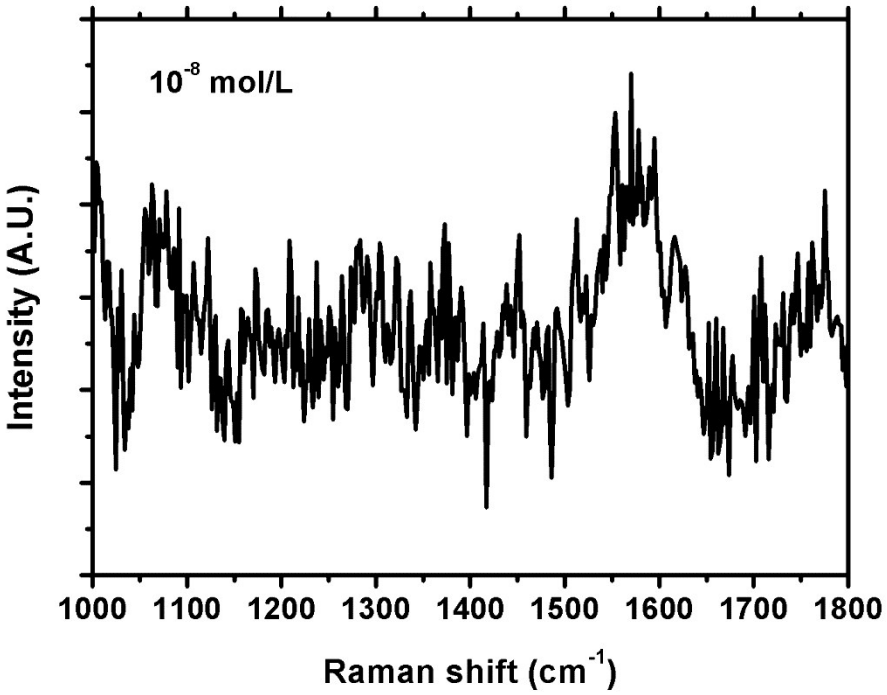

Fig. S10. The SERS spectrum of CoPt hollow NPs after adsorbing 4-MBA tip molecules from an extremely diluted solution with concentration of 10^{-8} mol/L.

	EF	Concentration limit	
Pt -based material SERS property without plasmonic metals	4.3×10^4	10^{-8}	Immobilization of Pt Nanoparticles via Rapid and Reusable Electropolymerization of Dopamine on TiO2 Nanotube Arrays for Reversible SERS Substrates and Nonenzymatic Glucose Sensors[1]
	1.4×10^3	——	Surface-Enhanced Raman Scattering on Aggregates of Platinum Nanoparticles with Definite Size[2]
	2.0×10^3	——	Electrochemical preparation of platinum nanothorn assemblies with high surface enhanced Raman scattering activity[3]
	0.5×10^3	——	SERS at Structured Palladium and Platinum Surfaces[4]
Pd -based material SERS property without plasmonic metals	1.5×10^3	——	Electrodeposition of Nanoflake Pd Structures: Structure-Dependent Wettability and SERS Activity[5]
	1.9×10^5	10^{-8}	Morphology dependent catalysis and surface enhanced Raman scattering (SERS) studies using Pd nanostructures in DNA, CTAB and PVA scaffolds[6]
	4.8×10^3	——	Electrodeposition of Triangular Pd Rod Nanostructures and Their Electrocatalytic and SERS Activities[7]
Bare Au SERS property	1.2×10^6	——	Fabrication of Au@Pt Multibranched Nanoparticles and Their Application to In Situ SERS Monitoring[8]
Pt or Pd-based material SERS property with plasmonic metals	6.0×10^5	——	Fabrication of Au@Pt Multibranched Nanoparticles and Their Application to In Situ SERS Monitoring[8]
	2.6×10^8	10^{-9}	Femtosecond Laser Direct Writing of Plasmonic Ag/Pd Alloy Nanostructures Enables Flexible Integration of Robust SERS Substrates[9]
	——	10^{-9}	Biogenic flower-shaped Au–Pd nanoparticles: synthesis, SERS detection and catalysis towards benzyl alcohol oxidation[10]
	3.0×10^3	——	A general seed-mediated approach to the synthesis of AgM (M @Au, Pt, and Pd) core–shell nanoplates and their SERS properties[11]
	2.5×10^3	——	Ag+-assisted heterogeneous growth of concave Pd@Au nanocubes for surface enhanced Raman scattering (SERS)[12]
	——	10^{-7}	Versatile synthesis of high surface area multimetallic nanosponges allowing control over nanostructure and alloying for catalysis and SERS detection[13]
Our work	$\sim0.5\times10^6$	10^{-7}	

Table. S1 SERS properties of Pt/Pd-based materials from previous reports, along with the data of CoPt hollow NPs in this work.

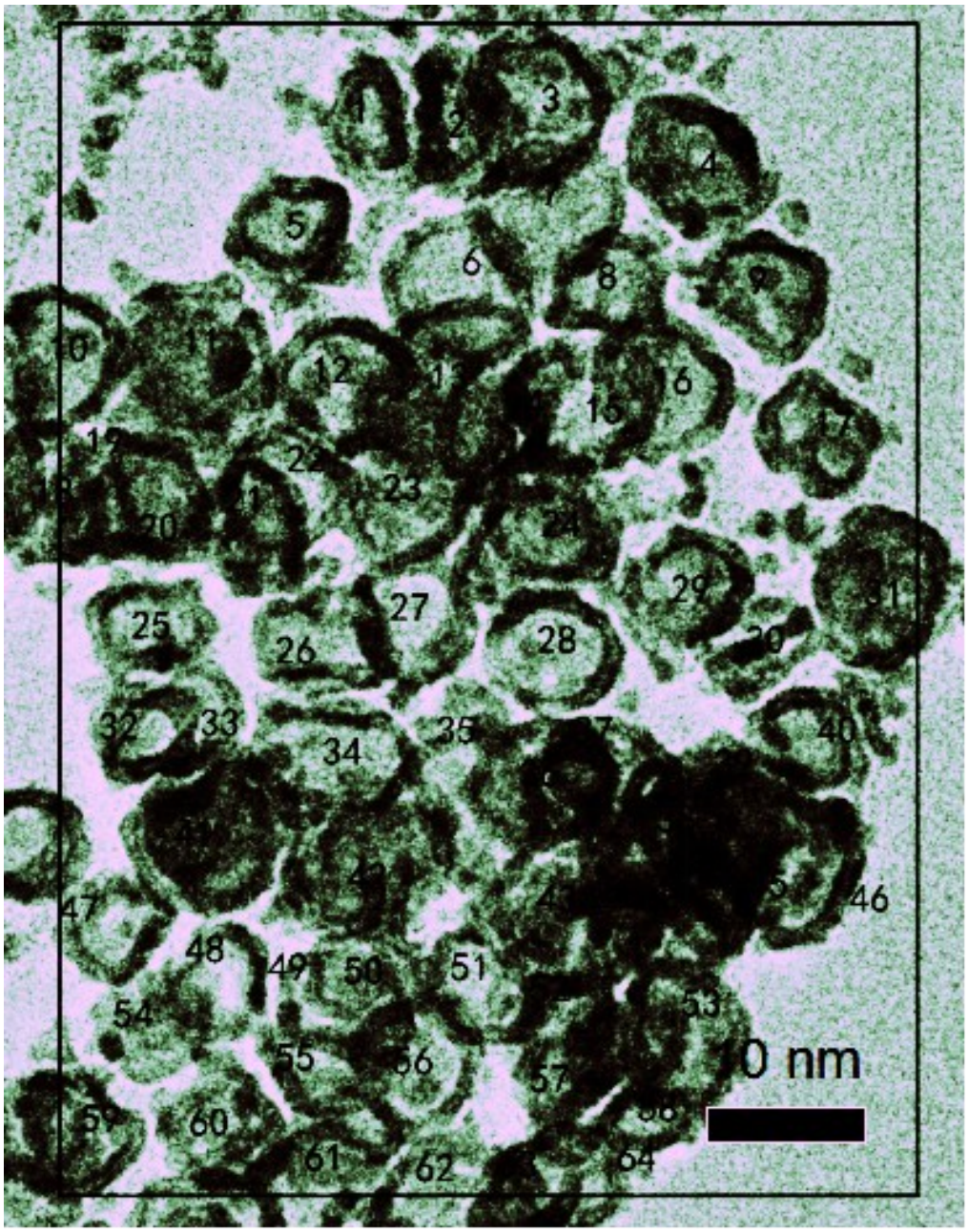

Fig. S11. TEM image of CoPt hollow NPs used to calculate the areal density, taken to be indicative of that on other substrates which were used for optical measurements.

The EF factor (G) was calculated to be approximately 0.5×10^6, according to the equation as following:

$$G= (I_{SERs}/N_{SERs})/(I_{bulk}/N_{bulk}),$$

where the number of tip molecules is represented as:

$$N_{SERs}=A\times N_{sub}\times A_{sub}/\sigma,$$

where A is the laser irradiation area (~1.5 μm^2), N_{sub} is the CoPt hollow NPs areal population (~1.6×10^{-2} nm^{-2}) and the diameter size (~8 nm) of the NPs was taken from Fig. S7; A_{sub} is the area of a single CoPt hollow NP (~200 nm^2), σ is the area of a single adsorbed 4-MBA molecule (~0.2 nm^2). It is assumed here that the substrate material surface was fully saturated with 4-MBA molecules and one monolayer was homogeneously deposited on the CoPt hollow NPs.

The number of tip molecules contributing to the Raman signal in the experiment was:

$$N_{\text{bulk}}=A\times h\times n_{bulk}=A\times h\times N_A\times\rho_{bulk}/M_{bulk},$$

where A is the laser irradiation area (~1.5 μm^2), h is the laser focusing depth (~10 μm), n_{bulk} is the number of tip molecules per unit volume, ρ_{bulk} is the density of bulk (~1.5 g/cm^3), M_{bulk} is the molecular weight of 4-MBA molecule (~154.19 g/mol), N_A is the Avogadro constant (~6.02×10^{23}).

This can be calculated as:

$$G = (I_{SERs}/N_{SERs})/(I_{bulk}/N_{bulk}).$$

Hence, the EF factor G is approximately 0.5×10^6.

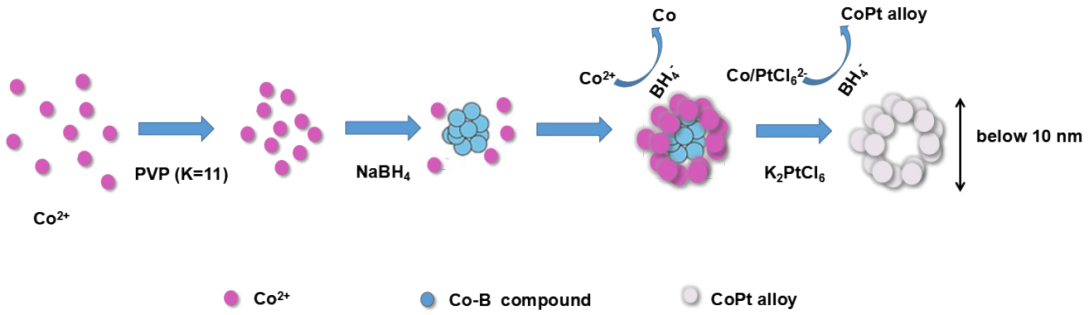

Scheme. S1 The illustration for the formation process of CoPt hollow NPs.

In the experimental process, Co atoms and Pt ions are involved in replacement reactions, leading to the formation of hollow nanostructures as illustrated in Scheme S1. At first, the short PVP chain aggregated Co ions, and facilitated the formation of small NPs. Secondly, Co ions were fast reduced, the Co-B compounds occur (a). And then, the Co-B nano-compounds became more and more, forming nanoparticles of amorphous Co-B nano-compounds, as depicted in step (b). At the same time, part of Co metal generated. After chloroplatinic ions were added, Pt ions were reduced at the expense of the Co in the Co–B compounds. Then Pt along with the co-reduced Co participated in the formation of CoPt nanocrystallite over the surface of Co–B compounds. With the additional acid corrosion effects on the Co–B nanocompounds, CoPt hollow alloys were formed as described in step (c). The chemistry is summarised by the equations below

$$2Co+PtCl_6=2Co^{2+}+Pt\downarrow+6Cl^- \text{ (a)}$$

$$BH_4^-+4Co^{2+}+8OH^-=4Co\downarrow+BO_2^-+6H_2O \text{ (b)}$$

$$2PtCl_6^{2-}+ BH_4^-+ 8OH^-=2Pt\downarrow+BO_2^-+6H_2O + 12Cl^- \text{ (c)}$$

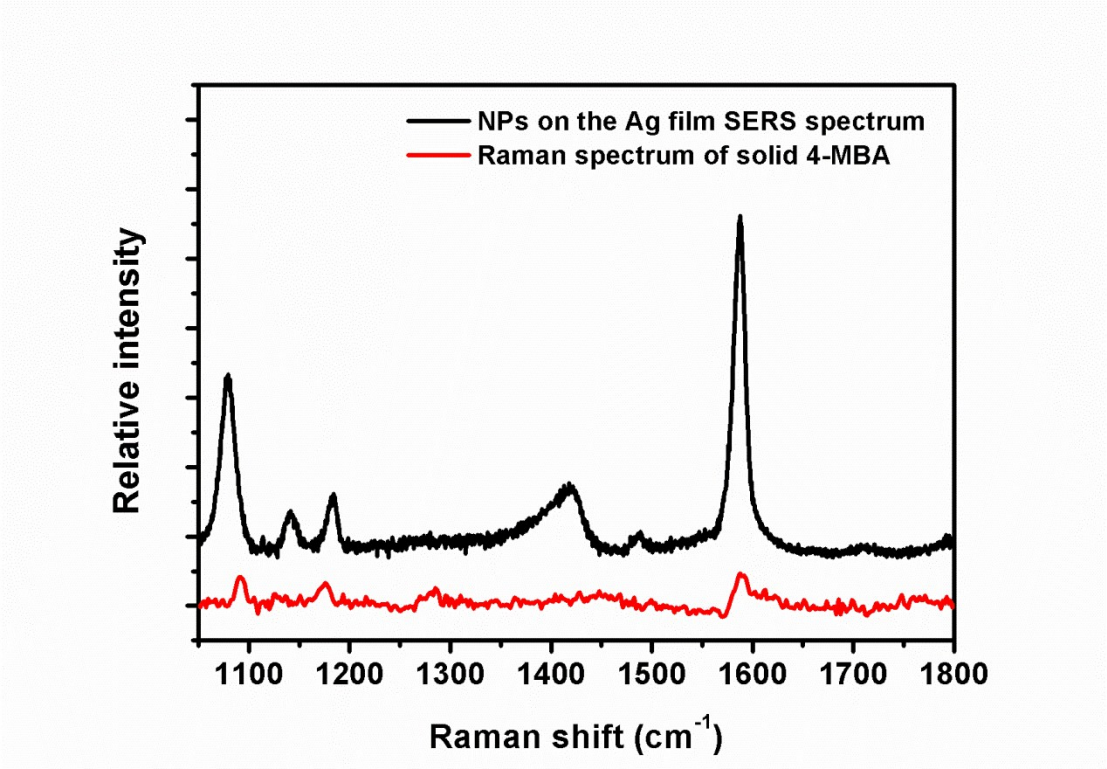

Fig.S12 Two SERS spectra from 4-MBA (10^{-2} mol/L) on the NPOM configuration and solid 4-MBA, respectively.

According to the equation as follows:

$$G= (I_{SERs}/N_{SERs})/(I_{bulk}/N_{bulk}),$$

the EF factor G is approximately ~2×10^6.

Reference:

1. J. Cai, J. Huang, M. Ge, J. Iocozzia, Z. Lin, K. Q. Zhang and Y. Lai, *Small*, 2017, 13.

2. K. Kim, K. L. Kim, H. B. Lee and K. S. Shin, *The Journal of Physical Chemistry C*, 2010, 114, 18679-18685.

3. N. Tian, Z. Y. Zhou, S. G. Sun, L. Cui, B. Ren and Z. Q. Tian, *Chem Commun*

(Camb), 2006, 4090-4092.

4. M. E. Abdelsalam, S. Mahajan, P. N. Bartlett, J. J. Baumberg and A. E. Russell, *Journal of the American Chemical Society*, 2007, 129, 7399-7406.

5. J. H. Shin, H. G. Kim, G. M. Baek, R. Kim, S. Jeon, J. H. Mun, H.-B.-R. Lee, Y. S. Jung, S. O. Kim, K. N. Kim and G. Y. Yeom, *RSC Advances*, 2016, 6, 70756-70762.

6. S. Kundu, S. I. Yi, L. Ma, Y. Chen, W. Dai, A. M. Sinyukov and H. Liang, *Dalton Trans*, 2017, 46, 9678-9691.

7. S. Choi, H. Jeong, K. H. Choi, J. Y. Song and J. Kim, *ACS Appl Mater Interfaces*, 2014, 6, 3002-3007.

8. Q. Cui, G. Shen, X. Yan, L. Li, H. Mohwald and M. Bargheer, *ACS Appl Mater Interfaces*, 2014, 6, 17075-17081.

9. Z.-C. Ma, Y.-L. Zhang, B. Han, X.-Q. Liu, H.-Z. Zhang, Q.-D. Chen and H.-B. Sun, *Advanced Materials Technologies*, 2017, 2, 1600270.

10. D. Sun, G. Zhang, X. Jiang, J. Huang, X. Jing, Y. Zheng, J. He and Q. Li, *J. Mater. Chem. A*, 2014, 2, 1767-1773.

11. S. Kumar-Krishnan, M. Estevez-González, R. Pérez, R. Esparza and M. Meyyappan, *RSC Advances*, 2017, 7, 27170-27176.

12. B. Jiang, L. Xu, W. Chen, C. Zou, Y. Yang, Y. Fu and S. Huang, *Nano Research*, 2017, 10, 3509-3521.

13. S. Tang, S. Vongehr, Y. Wang, J. Cui, X. Wang and X. Meng, *J. Mater. Chem. A*, 2014, 2, 3648-3660.